

Concentration Stratification and Crystal Dynamics in Solidifying Ammonium Chloride Solutions

Golshan Shayesteh ^a, Zhao Zhang ^b,
Mihaela Stefan-Kharicha ^a, Menghuai Wu ^a,
Abdellah Kharicha ^{a,c} and Andreas Ludwig ^{a*}

DOI: <https://doi.org/10.9734/bpi/mono/978-93-49473-95-9/CH1>

Peer-Review History:

This chapter was reviewed by following the Advanced Open Peer Review policy. This chapter was thoroughly checked to prevent plagiarism. As per editorial policy, a minimum of two peer-reviewers reviewed the manuscript. After review and revision of the manuscript, the Book Editor approved the manuscript for final publication. Peer review comments, comments of the editor(s), etc. are available here: <https://peerreviewarchive.com/review-history/3590.1>

ABSTRACT

Many alloys reveal an upwardly directed solutal buoyancy in the interdendritic mushy region as they solidify. Such a situation leads to a solute enrichment at the top of the melt pool and is prone to form segregation channels. Based on both experimental observations and numerical simulations applying an aqueous ammonium chloride solution subject to side cooling, this contribution discusses the complex interplay of different phenomena that leads to a sedimentation bed that is far from being homogenous. Concentration and flow stratification at the top part of the test cell, interdendritic flow channels transporting both segregated liquid and also crystal fragments into the bulk melt, crystal agglomerations that form at indentations observed at the exit of flow channels, and collapsing of crystal agglomerations and sliding down of mushy zone segments, all these phenomena lead to a highly unsteady solidification dynamic. These observations are relevant in fields such as metallurgy, materials science, geology, and environmental science and could enhance the design of industrial processes and contribute to natural system modeling.

Keywords: Solutal buoyancy; double-diffusive convection; crystal multiplication; macrosegregation; sedimentation.

^a Metallurgy Department, Montanuniversitaet Leoben, 8700 Leoben, Austria.

^b Primetals Technologies Limited, 4031 Linz, Austria.

^c CD Laboratory for Magnetohydrodynamic Application in Metallurgy, Montanuniversitaet Leoben, 8700 Leoben, Austria.

*Corresponding author: E-mail: ludwig@unileoben.ac.at;

1.1 INTRODUCTION

For over 50 years, flow-related phenomena that occur during solidification have been studied using aqueous ammonium chloride solutions ($\text{NH}_4\text{Cl-H}_2\text{O}$). With a hyper-eutectic composition, solidification starts with the formation of NH_4Cl crystals that reject H_2O . Therefore, the segregated interdendritic liquid is enriched in H_2O and thus lighter than the initial melt. Solutal buoyancy flow is the consequence. Copley et al. [1] investigated the origin of channels filled with equiaxed crystals, so-called freckles, during unidirectional solidification using $\text{NH}_4\text{Cl-H}_2\text{O}$ with 30 wt.% NH_4Cl . Their research concluded that freckles in solidified castings and ingots are caused by convection, whereby factors like density inversion, thermal and solute diffusivity, viscosity, and mushy zone curvature influence their occurrence. The formation and prevention of channels during solidification, particularly with aqueous ammonium chloride solution, were investigated in the 1980s by Sample and Hellawell [2,3]. Their research implicitly delved into double-diffusive convection during the solidification process. The study aimed to comprehend the mechanisms involved in the creation and propagation of channels. Various experimental setups were used, including a stationary mold, a vertical mold, an inclined mold (at angles between 20 and 30 degrees), and a rotating mold [2,3]. In 1988/89, Beckermann and Viskanta [4–6] and Christenson and Incropera et al. [7,8] studied the solidification/melting of $\text{NH}_4\text{Cl-H}_2\text{O}$ solutions in rectangular cavities. They showed that solutally driven flow strongly influences solidification rates, localized remelting, and macroscopic solute redistribution. They showed that with side-cooling of such a solution, solidification happens along the cooled sidewall while a variety of double-diffusive convection phenomena in the liquid occur, including layers, plumes, and stable concentration stratifications. Even remelting in parts of the system could be observed.

Chen and Chen [9] conducted a comprehensive overview of channel and freckle formation during directional solidification of $\text{NH}_4\text{Cl-H}_2\text{O}$. Their study focused on the presence of plumes in the fluid region just above the mushy zone, particularly under conditions of a large temperature gradient. The researchers utilized computed tomography to estimate parameters such as mushy zone porosity. Additionally, they examined factors like the solute Rayleigh number, channel inner diameter, average dendrite size, and average flow velocity in the deeper mushy zone regions. Shih and Tu [10] conducted extensive research to comprehend double-diffusive convection during solidification in hypereutectic $\text{NH}_4\text{Cl-H}_2\text{O}$ alloys. Using particle image velocimetry (PIV), they measured flow fields and observed several flow circulation rolls near the mushy zone and in the melt for two concentrations (25 wt.% and 28 wt.%). Additionally, Shih et al. [11] explored lid-driven flow experiments to mitigate freckle formation. They measured temperature and concentration during solidification, finding that reducing the temperature and concentration gradient led to a decrease in the number of freckles. The experimental results indicated that increasing the slider speed effectively suppressed the development of double-diffusive convection. Kharicha et al. [12,13] conducted experiments to monitor flow dynamics during the solidification of the $\text{NH}_4\text{Cl-H}_2\text{O}$ solution using PIV. Peppin et al. [14] found that the formation of plumes can be suppressed if the freezing rate is increased. Recently, Thakur et al. [15,16] used dual-wavelength interferometry to simultaneously measure temperature and salt concentration

distributions during unidirectional solidification of $\text{NH}_4\text{Cl-H}_2\text{O}$ solutions. Various subprocesses that result in the formation of the stepped structure of solutal-thermal gradients were mapped through rainbow-schlieren deflectometry and flow velocities have been quantified using PIV. Zhong et al. [17] used a larger cylindrical cell to observe the sinking of equiaxed crystals and the formation of a sedimented layer of crystals. They called the massive crystal sedimentation from the cooled top 'crystal rain' similar to the 'showering from the surface' as reported in ref. [18]. In this case, the amount of sedimenting crystals was so high that columnar growth from the bottom was stopped and a columnar-to-equiaxed transition (CET) occurred.

A numerical modelling study is beneficial to comprehensively understand the flow regimes that are linked to the development of the solidifying mushy zone and the formation of macrosegregation. Relying solely on in-situ observed experimental information is deemed inadequate as important quantities like local composition variations can optically not be captured using $\text{NH}_4\text{Cl-H}_2\text{O}$ solutions. Numerical modeling serves as an important tool for simulating and analyzing the dynamics inherent in solidification processes. Beckermann and Viskanta [4,6] conducted both numerical and experimental investigations of double-diffusive convection during solidification. Their studies revealed that the remelting of columnar dendrites could be a contributing factor to the formation of channels. Kharicha et al. [19] introduced a 2D cellular automaton model to investigate double-diffusive convection during the solidification of binary alloys. To accurately capture the smallest solute plumes, the solidification model simulates the envelope of columnar dendrites using a cellular automaton model. Their study identified various flow regimes, with the turbulent regime being specifically associated with the generation of individual plumes at each columnar dendrite. Wu et al. [20] conducted a comprehensive two-part study on solidification of an $\text{NH}_4\text{Cl-H}_2\text{O}$ solution. In the first part, they employed a dendritic solidification model to reproduce an experimentally monitored transient flow. A quantitative agreement was observed between the simulated and experimental results. The second part focused on the interaction between flow and solidification, correlating flow regimes with mushy zone solidification quantities.

In the present contribution, experimental observations are opposed to numerical results. After describing the experimental procedure, the numerical model is briefly sketched. In the main part of this work, some experimental results are presented, followed by the outline of the numerical predictions. It turned out that the simplified numerical model helps to better understand the physical processes that lead to the formation of interdendritic flow channels and the concentration and flow stratification at the top of the test cell. However, the experiment reveals additional phenomena that are not accounted for by the model. Thus, the corresponding limitations of the numerical model are discussed while further details on the uneven sedimentation at the bottom of the test cell are given.

1.2 EXPERIMENTAL PROCEDURE

A 62.6°C hot NH₄Cl-H₂O solution with 32.5 wt.% NH₄Cl was cast into a relatively large, preheated test cell with a clear height of 60 cm, width of 40 cm, and thickness of 6 cm. For the presented experiments, the resulting bath height was 42 cm. The test cell consisted of water-cooled sidewalls made of brass and two plexiglass sheets as the front and rear windows. The bottom plate was also brass but without any active cooling system. Cooling of the sidewalls was done by pumping water as a coolant through meander-type flow channels which were machined inside the brass. The temperature of the coolant was governed by an external cooling bath. The solution was fabricated by dissolving NH₄Cl that had a purity of +99.7 pct in distilled water. After removing some bubbles that had adhered to the plexiglass windows, the test cell was covered with a glass sheet and the cooling on the sidewalls was activated. Fig. 1.1 shows corresponding cooling curves together with a picture of the containment at the end of the experiment at around 12000 s after the start of the cooling. To avoid condensation of air moisture at the windows, $T_{inf} = 278$ K (5 °C) was chosen as the minimal cooling temperature. This temperature is around 20.7°C above the eutectic temperature at which the solution would completely solidify. Therefore, the solution was only partly solidified at the end of the experiment. We have performed the same experiment two times, one time with a permanent light source and a Canon EOS R6 camera and the second time with a flash-light illumination by using a Nd: YAG laser and a standard CCD camera. In this contribution, we will present and discuss only optical observations that were made during these two runs.

The liquidus temperature of the NH₄Cl-H₂O alloy deployed in these experiments was $T_l = 318$ K (45 °C). As demonstrated in Fig. 1.1a, cooling was at a nearly constant rate of 0.8 K/min. At 1350 s after cooling had commenced, the temperature of the brass walls fell below T_l . Visible crystals at the sidewalls formed approximately 150 s later.

1.3 NUMERICAL APPROACH

To simulate the above-described experiment, the following assumptions and simplifications were made.

- The numerical approach considered only two hydrodynamic phases: liquid and dendritic solid. The solid could not move. For the liquid phase, thermo-solutal buoyancy is considered. The formation of equiaxed crystals or crystal fragments was neglected. The model does not consider melting. Further model details can be found in [20].
- The numerical simulation was only 2D, with a uniform initial temperature distribution and a liquid that was initially at rest.
- The numerical domain had the height of the bath (42 cm) but only a width of 10 cm. As boundary conditions adiabatic walls have been assumed except the cooled sidewall.

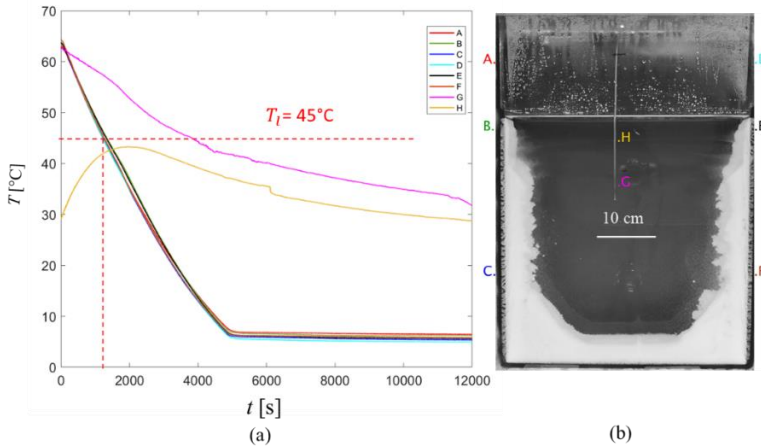


Fig. 1.1. (a) Typical temperature curves as recorded during the experimental run with a 32.5 wt.% $\text{NH}_4\text{Cl-H}_2\text{O}$ solution. Temperatures were measured with 6 thermocouples on the brass surfaces at different positions (A, B, C, D, E, F), inside the cell (G) and outside with contact to the plexiglass window (H). (b) Centered view of the test cell at the end of the experimental run together with the positions of the thermocouples

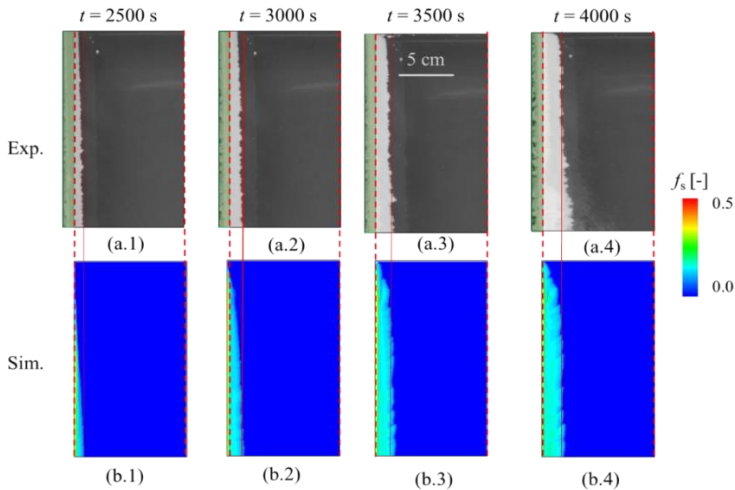


Fig. 1.2. Comparison of the evolution of the mushy layer at the top of the bath

The upper row shows the experimental observations, and the lower row the numerical pendants. This comparison was done to fix the heat transfer from the alloy to the brass sidewall

The boundary condition at the cold sidewall was chosen such that the thickness of the predicted mushy layer for the case without flow corresponds to the experimentally observed thickness at the upper region of the bath for four different points in time. A suitable heat transfer coefficient $H = 700 \text{ W/m}^2/\text{K}$ was proved necessary. In Fig. 1.2 the experiment is compared to a simulation that considered flow. Although the experimental observations were made from an inclined angle to the sidewall (a.1-a.4), the simulated mushy layer thickness shows sufficient accordance (b.1-b.4).

The material properties were taken according to Table 1.1.

Table 1.1. Materials properties used for the numerical approach

Contents	Symbol	Values	References
Composition	C_0	32.5 wt.%	-
Pouring temperature	T_p	335.8 K	-
Liquidus temperature	T_l	318.15 K	[21]
Solidus temperature	T_s	257.6 K	[21]
Liquidus slope	m	476.2 K/wt.%	[21]
Equilibrium partition coeff.	k	2.38	[20,22]
Primary dendritic arm spacing	l_1	600 μm	[20]
Secondary dendritic arm spacing	l_2	100 μm	[20]
Liquid density (reference density)	ρ_l	1073 kg/m^3	[21]
Viscosity of melt	μ_l	$1.3 \cdot 10^{-3} \text{ kg}/(\text{m} \cdot \text{s})$	[22]
Specific heat	C_p	3249 $\text{J}/(\text{kg} \cdot \text{K})$	[21]
Latent heat	L	$3.18 \cdot 10^5 \text{ J}/\text{kg}$	[20]
Thermal conductivity of the melt	k_l	$0.468 \text{ W}/(\text{m} \cdot \text{K})$	[20]
Thermal conductivity of the solid	k_s	$2.7 \text{ W}/(\text{m} \cdot \text{K})$	[20]
Thermal expansion coefficient	b_T	$3.9 \cdot 10^{-4} \text{ K}^{-1}$	[20]
Solute expansion coefficient.	b_C	$2.87 \cdot 10^{-3} \text{ wt.}\%^{-1}$	[20]
Diffusion coefficient. in the liquid	D_l	$4.8 \cdot 10^{-9} \text{ m}^2/\text{s}$	[22]
Diffusion coefficient in the solid	D_s	0	-

1.4 RESULTS AND DISCUSSION

Experimental results: Approximately 1350 s following the onset of cooling, the temperature sensors embedded in the brass sidewalls attained the liquidus temperature. At almost 1500 s, the initial crystals became apparent within a gap between the brass sidewall and the plexiglass, and shortly thereafter, crystals also emerged on the surface of the sidewalls. Upon reaching this point, the brass reached a temperature of 2 K below the liquidus. After an additional 900 s, the entire surface of the brass was entirely coated with solid material. During this

stage, no solid material formed at the bottom, and there were no crystals observable in the bulk melt.

Moving crystals appeared in the lower corner regions around 2400 s after the onset of cooling. After another 600 s, the bottom of the test cell was entirely coated with crystals. At approximately 4300 s after the cooling started, there was a noticeable increase in the interaction between the flow along the vertical mushy layer that had formed on the left and right sidewalls. The presence of large-scale vortices and evident continuity in crystal movement across both cooled sides of the test cell led to the volatile motion of the crystals. Fig. 1.3a-c indicates areas of rapid crystal sedimentation, clouds of crystals, and regions where the crystal motion is less distinct. The sedimentation layer at the bottom increases noticeably from Fig. 1.3a to Fig. 1.3c. The corresponding video demonstrates that sedimentation of crystals does not happen regularly by individual crystals, but rather by cloud-like "crystal avalanches" occurring again and again. They were caused by two different mechanisms outlined in §4.3. In Fig. 1.3e-f, pictures that were taken with a PIV camera and a laser flashlight illumination, show two mushy zone details (highlighted with the yellow ellipses) that disappeared between $t = 6000$ and 7000 s. These structures detached from the mushy region and sedimented downward to the bottom region (highlighted with the blue ellipse in Fig. 1.3e). Note that the pictures shown in Fig. 1.3 were taken from two different but similar experiments. Using a standard camera and a permanent light source (Fig. 1.3a-c) different details can be seen compared to a PIV camera and a laser flashlight illumination (Fig. 1.3d-f). Especially, with the second method, interdendritic flow channels and different sedimentation layers become more clearly visible. However, the interdendritic flow channels can also be guessed by the first method.

Finally, it is worth mentioning that at the top of the bath, the flow differs from the rest of the melt. In Fig. 1.3a-c, the flow carries clouds of tiny crystals horizontally from left to right and vice versa. Such meandering flow patterns have been reported in previous solidification experiments using aqueous ammonium-chloride solutions [6–8,13]. This flow pattern developed approximately 4600 s after cooling commenced and lasted until the end of the experiment. Therefore, the effect is also visible in Fig. 1b.

Numerical results: Fig. 1.4 and Fig. 1.5 show the evolution of the solid fraction, liquid velocity, and liquid concentration as calculated numerically. When cooling starts, the melt in the vicinity of the sidewall begins to flow downwards as a result of thermal buoyancy. At around 1500 s after the start of the cooling, the first solid covers the cooled sidewall. Fig. 1.4a shows that at this initial stage of solidification, the flow along the sidewall still maintains a downward trajectory, leading to a slightly colder and thus marginally greater solid fraction at the lower end of the sidewall. While the amount of solid fraction increases with time, the interdendritic liquid becomes segregated with H_2O (Fig. 1.5b) and thus starts to rise. In Fig. 1.4b, the thermally induced downward flow is redirected by the solutally induced upward flow, at approximately 1/3 of the height. The corresponding stagnation point is gradually rising.

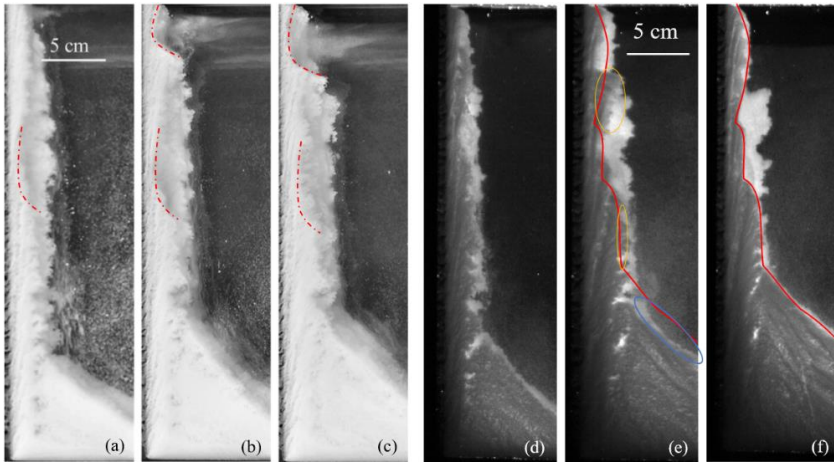


Fig. 1.3. Evolution of solid fraction from two similar experiments for different points in time. (a-c) first experiment with pictures taken with a standard camera and a permanent light source at (a) 5000 s, (b) 6000 s, and (c) 7000 s. (d-f) second experiment with pictures taken with the PIV camera and illuminated by a single laser flash also at (d) 5000 s, (e) 6000 s, and (f) 7000 s. In (a-c) indentations (bowl-shaped depressions) in the vertical mushy layer are marked with red dot-dashed lines. In (e-f) the red line indicates the 'dark grey' edge of the mushy layer shown in (f). Yellow ellipses in (e) show mushy segments that are missing in (f) and the blue ellipse shows a region that is empty in (e) but filled in (f)

Around 3000 s, the flow along the sidewall ascends entirely, maintaining relative stability across the entire mushy layer, Fig. 1.4d. In contrast, the corresponding downward flow in the bulk melt has become unsteady, with many volatile vortices. The driving force behind this phenomenon is twofold: mass conservation and domain walls compel the liquid downward, while the downward-flowing liquid, enriched in H₂O (green in Fig. 1.5d), tends to ascend due to slight segregation. This ambiguous condition exists in several regions in the bulk melt. The bulk melt has to descend as it must close the loop with the strongly rising interdendritic solutal buoyancy flow. Slightly segregated liquid manages to rise at certain points, resulting in the formation of vortices.

At 4000 s after the start of the cooling (Fig. 1.4e), these vortices are arranged into five, and later at 5000 s (Fig. 1.4f), into six distinct regions or layers. Fig. 1.5e-f reveals that these layers are defined by a certain degree of solute concentration. A flow and composition stratification, like the one described here, is characteristic of a double-diffusive convection scenario. In the present case, an anti-clockwise vortex in each layer transports solute from the edge of the mushy layer into the bulk melt. The concentration level at the bottom of the layer is therefore somewhat higher compared to the top of the layer. As solidification in the mushy zone proceeds, the edge of the two-phase front represents a continuous source of solute

elements. Hence, the layers become gradually more densely concentrated and grow, while the vortex becomes weaker. At 4000 s these layers are inclined towards the top of the domain, but later at 5000 s they become horizontal. Furthermore, the different layers gradually descend. This is caused by the fact that the top stratified layer is constantly fed by H₂O-enriched liquid from the solidifying mushy zone (Fig. 1.5e-h) and thus markedly grows thereby pushing the lower layers down. Essentially, Fig. 1.5e-h shows the formation of a new (dark brown) and the separation of an existing layer (light brown).

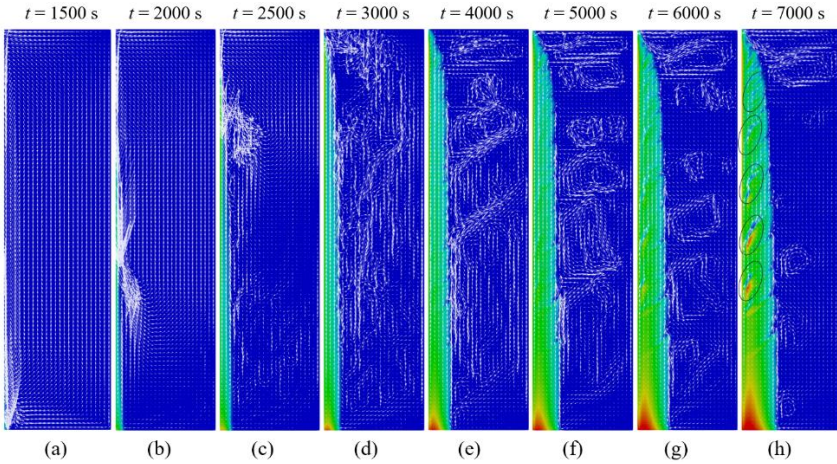


Fig. 1.4. Evolution of solid fraction overlaid with the liquid velocity vectors. The blue color represents areas without solid and the red color those with a volume fraction of more than 50%. The arrows represent velocities from 0 mm/s to V_{max} , with $V_{max} = 9.6$ mm/s (a), 9.5 mm/s (b), 7.0 mm/s (c), 2.2 mm/s (d), 1.2 mm/s (e), 0.94 mm/s (f), 0.7 mm/s (g) and (h)

Besides the development of the flow and composition stratification, the appearance of flow channels in the mushy zone is another significant numerical result. In Fig. 1.4h and Fig. 1.5h, five flow channels have been highlighted. They are rather equally separated and reveal a similar inclination towards the bulk melt. By such flow channels, the segregated interdendritic liquid leaves the vertical mushy zone, Fig. 1.5h. The explanation for the formation of flow channels is the following. While the segregated interdendritic liquid is moving through the mushy zone, it interferes with the local solidification process; exchanging the interdendritic liquid with less segregated melt leads to further solidification, exchanging the interdendritic liquid by more segregated liquid leads to less solidification (or even remelting). As a concentration gradient across the mushy zone in the interdendritic liquid exists with higher segregated melt for larger solid fractions and lower for smaller, a flow component in the direction of this gradient will lead to a change in the local solidification dynamic. This is the reason why solid fraction variations in the mushy layer develop. What causes the beginning of such variations is the subject of ongoing discussions in the community. Pertinently, a local solid fraction reduction rapidly

develops into a flow channel, and so the process is self-enforcing because the channels are pointing upward with some inclination away from the sidewall. Thus, the flow of higher-segregated melt is redirected towards an area of lower solid fraction. When the flow in the channel intensifies, it pulls interdendritic liquid from beneath towards the channel. That results in a flow component in the direction of the sidewall and thus to a localized amplified solidification as can be seen by the red areas below two of the channels highlighted in Fig. 1.4h.

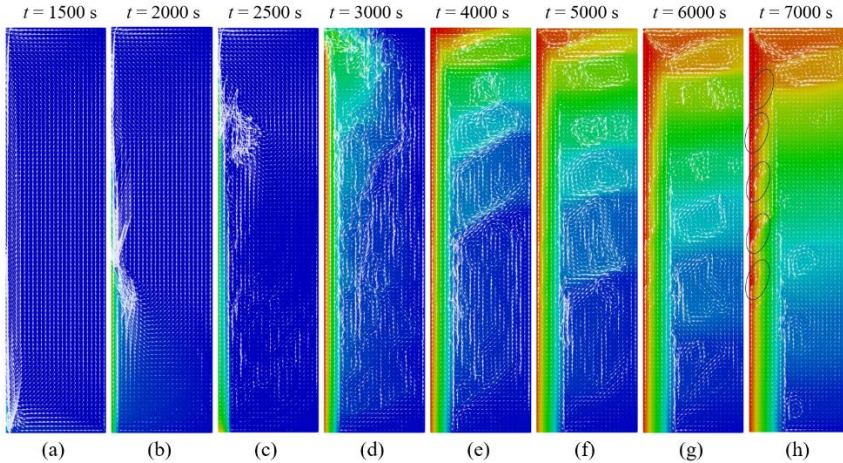


Fig. 1.5. Evolution of the liquid concentration overlaid with the liquid velocity vectors. The blue color represents the initial 32.5 wt.% NH_4Cl (67.5 wt.% H_2O) whereas the red color shows liquid with less than 25.0 wt.% NH_4Cl (more than 75 wt.% H_2O)

Interaction of the flow inside and outside of the mushy zone causes localized variation in the solid fraction at the edge of the mushy zone. Here, it is simple to adapt the local concentration by a flow component point towards or away from the mushy zone edge. Analysis of the top part of Fig. 1.4e-h reveals that such local solid fraction variations at the mushy zone edge can also further develop into larger channels that allow the melt to dissipate from the mushy zone. The top highlighted channel in Fig. 1.4h is of that type. However, the remaining four highlighted channels in Fig. 1.4h do not have (yet) a dedicated flow exit from the mush. They have developed fully inside the dendritic skeleton.

Comparison of numerical results with observations: The numerical approach reveals three major differences compared to the experiment. The first and most grave difference is that no equiaxed crystals are considered in the simulation. Second, the simulation considers a domain that had the correct height, but a reduced width of only 10 cm rather than the 40 cm of the test cell. Finally, the simulation is only two-dimensional whereas the real process happened in a test cell that had a clear thickness of 6 cm. All these differences have significant implications. Nevertheless, the simulation still helps to better understand some of the physical

processes that occurred during the experiment, in particular, the formation of flow channels in the mushy zone and the formation of the flow stratification at the top of the domain.

In Fig. 1.3 a-c, flow channels appear as thin dark lines and, in Fig. 1.3d-f, as bright lines. These flow channels are located directly at the front window. Flow channels in the center of the cell's width are not visible. The plexiglass window influences the temperature distribution inside the test cell, and close to the window, the temperature might be different from the 2D simulation, where lateral heat loss was neglected. However, the physical mechanism for the formation of a flow channel as described in [2,3] and as also reproduced by the numerical results is still what causes the channel to form. Also, flow stratification at the top of the test cell confirms the occurrence of an upwards-pointing interdendritic solutal buoyancy flow. In Fig. 1.3a-c, and also in Fig. 1.1b, it can be seen that a horizontal flow field carries clouds of tiny crystals from left to right and vice versa. This kind of meandering flow pattern is known from the literature [6–8] and also predicted by the simulation. It is caused by flow and composition stratification also known as double-diffusive convection. The fact that the simulation does not account for the clouds of tiny crystals that travel with the stream indicates that those clouds are of minor importance for this flow phenomenon to occur.

Our experiment suggests that crystals, or more precisely crystalline fragments, constantly flow out of the top part of the vertical mushy layers, presumably also ejected from the interdendritic flow channels [23–27]. This important observation can of course not be caught by the simplified simulation. However, the larger crystals in the bulk melt that are mainly sedimenting but are also swirling around with the vortices, do have a great impact on the extension of the stratification. Fig. 1.5 demonstrates that flow and composition stratification signify a clearly defined flow pattern. The unsteady flow pattern in the experiment does not allow the stratified flow pattern to further evolve downwards. Therefore, stratification is restricted to the top part of the bath (Fig. 1.3a-c). The stratification only proceeds further downwards when most of the crystals have sedimented.

Another important topic is the local remelting of the vertical mushy zone at the exit region of a flow channel. Here, indentations (bowl-shaped depressions) form at the edge of the vertical mushy layer. They are marked with red dot-dashed lines in Fig. 1.3a-c. The occurrence of such indentations and corresponding implications on the solidification dynamics is described in more detail in another publication of the present authors [28]. As the numerical model does not account for melting, this phenomenon is numerically not described.

Finally, it must be discussed that areas of mushy zone segments frequently slide downwards. The simulation cannot capture this phenomenon, as the solid is assumed to be always fixed in the same space. However, the numerical results presented in Figs. 1.4 and 5 show that local retardation of solidification (and in reality even remelting) is associated with the occurrence of flow channels. If those areas are located close to the edge of the mushy zone, loosened segments might slide downwards. Sliding down of larger crystal debris also happens when sinking

crystals stick on protruded mushy zone structures, and agglomerate until the agglomeration collapses because of its increasing size. When those crystal agglomerations tumble down, they collide with the mushy zone further down. As a result, crystal multiplication and clouds of fragments occur, as shown in Fig. 1.3a by the many unfocused crystals. Also, the disappearance of parts from the mushy zone formally located below an overhanging segment, as shown in Fig. 1.3e by the two yellow ellipses, can be understood.

1.5 CONCLUSIONS

Although the presented numerical approach reveals severe restrictions that make a direct comparison with the experiments impossible, the simulation still helps to improve understanding of important process details. Upwards pointing solutal buoyancy flow in the vertical mushy zone gradually increases the concentration at the top of the test cell. This leads to flow and concentration stratification as known from other double-diffusive flow scenarios. However, the stratification layers cannot evolve downwards as flow vortices in the bulk melt interfere with the defined flow pattern of the stratified layers.

As the interdendritic liquid ascends, the interplay between flow instability and the solidification process leads to localized regions where solidification is hindered. These areas are the origin of flow channels. Under the present process conditions, several flow channels form, both predicted by the simulation and also observed in the experiments. They all reveal a slight inclination towards the bulk melt. The flow channels transport not only segregated liquid into the bulk melt but also crystalline fragments. Clouds of tiny crystals/fragments follow the liquid flow and so enable the observation of the flow stratification in the upper part of the test cell. Larger crystals/fragments directly sink and flow along the edge of the vertical mushy zone. Flow channels that leave the mushy zone somewhere in the upper part of the test cell, form indentations (bowl-like depressions) at the edge of the mushy layer. As higher segregated melt permanently interferes with the solid skeleton, these indentations also change with time. By local melting and agglomerating crystals that sink along the edge of the mushy zone, they can either grow or diminish in size.

Crystals that stuck at these indentations, but also at protruded mushy zone segments, form crystal agglomerations. Those agglomerations collapse when getting too large. It is even possible that the segregated melt from the flow channels directly melts away mushy zone segments, that slide down when getting loose. Collapsing crystal agglomerations and loosened mushy zone segments lead to further fragmentation and crystal multiplication when impacting the mushy layer underneath. These phenomena occur frequently in the experiment. As a consequence, uneven layering of the crystal sediment at the bottom of the test cell occurs.

The observations show that in technical processes, but also in processes that occur in nature, the occurrence of uneven structures might be caused by a complex interplay of different phenomena. Here, flow and concentration stratification, segregation channels, collapsing of crystal agglomerations/mushy zone segments,

and unsteady flow vortices lead to a sedimentation bed that is far from being homogenous.

CONFERENCE DISCLAIMER

Abstract part of this manuscript was previously presented at the conference: The 8th International Conference on Solidification and Gravity dated from 02 th September to 05th September 2024 in Miskolc - Lillafüred, Hungary, Web Link of the proceeding: <https://www.solgrav.uni-miskolc.hu/SG24-Program&Abstracts.pdf>.

DISCLAIMER (ARTIFICIAL INTELLIGENCE)

The authors hereby declare that NO generative AI technologies such as Large Language Models (ChatGPT, COPILOT, etc.) and text-to-image generators have been used during the writing or editing of this manuscript.

ACKNOWLEDGEMENTS

The authors would like to express their gratitude to the Montanuniversitaet Leoben for sponsoring this work in the framework of the recent doctoral program.

COMPETING INTERESTS

Authors have declared that no competing interests exist.

REFERENCES

1. S.M. Copley, A.F. Giamei, S.M. Johnson, M.F. Hornbecker, M. Copley, The Origin of Freckles in Unidirectionally Solidified Castings, *Met. Trans.* 1 (1970) 2193–2204.
2. A. Sample, A. Hellawell, The effect of mold precession on channel and macro-segregation in ammonium chloride-water analog castings, *Metall. Trans. B.* 13 (1982) 495–501. <https://doi.org/10.1007/BF02667766>.
3. A. Sample, A. Hellawell, Mechanisms of Formation and Prevention of Channel Segregation During Alloy Solidification., *Metall. Trans. A, Phys. Metall. Mater. Sci.* 15 A (1984) 2163–2173. <https://doi.org/10.1007/bf02647099>.
4. C. Beckermann, R. Viskanta, Double-diffusive convection due to melting, *Int. J. Heat Mass Transf.* 31 (1988) 2077–89. [https://doi.org/10.1016/0017-9310\(88\)90118-4](https://doi.org/10.1016/0017-9310(88)90118-4).
5. C. Beckermann, R. Viskanta, An experimental study of melting of binary mixtures with double-diffusive convection in the liquid, *Exp. Therm. Fluid Sci.* 2 (1989) 17–26. [https://doi.org/10.1016/0894-1777\(89\)90045-9](https://doi.org/10.1016/0894-1777(89)90045-9).
6. C. Beckermann, R. Viskanta, An experimental study of solidification of binary mixtures with double-diffusive convection in the liquid, *Chem. Eng. Commun.* 85 (1989) 135–156. <https://doi.org/10.1080/00986448908940352>.

7. M.S. Christenson, F.P. Incropera, Solidification of an aqueous ammonium solution in a rectangular cavity- I. Experimental study, *Int. J. Heat Mass Transf.* 32 (1989) 47–68. [https://doi.org/10.1016/0017-9310\(89\)90090-2](https://doi.org/10.1016/0017-9310(89)90090-2).
8. M.S. Christenson, W.D. Bennon, F.P. Incropera, Solidification of an aqueous ammonium chloride solution in a rectangular cavity- II. Comparison of predicted and measured results, *Int. J. Heat Mass Transf.* 32 (1989) 69–79. [https://doi.org/10.1016/0017-9310\(89\)90091-4](https://doi.org/10.1016/0017-9310(89)90091-4).
9. C.F. Chen, F. Chen, Experimental study of directional solidification of aqueous ammonium chloride solution, *J. Fluid Mech.* 227 (1991) 567–586. <https://doi.org/10.1017/S0022112091000253>.
10. Y.C. Shih, S.M. Tu, PIV study on the development of double-diffusive convection during the solidification effected by lateral cooling for a super-eutectic binary solution, *Appl. Ther. Eng.* 29 (2009) 2773–2782. <https://doi.org/10.1016/j.applthermaleng.2009.01.012>.
11. Y.C. Shih, S.M. Tu, C.C. Chiu, Suppressing freckles during solidification due to periodic motion of top liquid layer, *Appl. Ther. Eng.* 50 (2013) 1055–1069. <https://doi.org/10.1016/j.applthermaleng.2012.08.059>.
12. A. Kharicha, M. Stefan-Kharicha, A. Ludwig, M. Wu, Simultaneous Observation of Melt Flow and Motion of Equiaxed Crystals During Solidification Using a Dual Phase Particle Image Velocimetry Technique. Part I: Stage Characterization of Melt Flow and Equiaxed Crystal Motion, *Met. Mater. Trans. A.* 44 (2013) 650–660.
13. A. Kharicha, M. Stefan-Kharicha, A. Ludwig, M. Wu, Simultaneous Observation of Melt Flow and Motion of Equiaxed Crystals During Solidification Using a Dual Phase Particle Image Velocimetry Technique. Part II: Relative Velocities, *Met. Mater. Trans. A.* 44 (2013) 661–668. <https://doi.org/10.1007/s11661-012-1415-y>.
14. S.S.L. Peppin, H.E. Huppert, M.G. Worster, Steady-state solidification of aqueous ammonium chloride, *J. Fluid Mech.* 599 (2008) 465–476. <https://doi.org/10.1017/S0022112008000219>.
15. I. Thakur, S. Karagadde, A. Srivastava, *Phys. Rev. Fluids* 7 (2022) 063501/1–27.
16. I. Thakur, S. Karagadde, A. Srivastava, Mechanisms leading to the formation of double-diffusive layers during unidirectional solidification of aqueous NH₄Cl solution, *Phys. Rev. Fluids.* 7 (2022) 063501/1–27. <https://doi.org/10.1103/PhysRevFluids.7.063501>.
17. H. Zhong, Y. Zhang, X. Chen, C. Wu, Z. Wei, Q. Zhai, In situ observation of crystal rain and its effect on columnar to equiaxed transition, *Metals (Basel)*. 6 (2016) 271/1–9. <https://doi.org/10.3390/met6110271>.
18. J. Hutt, D. StJohn, The origins of the equiaxed zone -Review of theoretical and experimental work, *Int. J. Cast Met. Res.* 11 (1998) 13–22. <https://doi.org/10.1080/13640461.1998.11819254>.
19. A. Kharicha, M. Stefan-Kharicha, M. Wu, A. Ludwig, Exploration of the double-diffusive convection during dendritic solidification with a combined volume-averaging and cellular-automaton model, *IOP Conf. Ser. Mater. Sci. Eng.* 33 (2012) 012115. <https://doi.org/10.1088/1757-899X/33/1/012115>.
20. M. Wu, M. Stefan-Kharicha, A. Kharicha, A. Ludwig, A numerical study on solidification of NH₄Cl – 70 wt .% H₂O solution in a water-cooled mould

- with a large sample thickness, *Int. J. Heat Mass Transf.* 164 (2021) 120566. <https://doi.org/10.1016/j.ijheatmasstransfer.2020.120566>.
21. M. Stefan-Kharicha, A. Kharicha, J. Mogeritsch, M. Wu, A. Ludwig, Review of Ammonium Chloride-Water Solution Properties, *J. Chem. Eng. Data.* 63 (2018) 3170–3183. <https://doi.org/10.1021/acs.jced.7b01062>.
 22. C.M.G. Rodrigues, M. Wu, H. Zhang, A. Ludwig, A. Kharicha, Validation of a Capillary-Driven Fragmentation Model During Mixed Columnar-Equiaxed Solidification with Melt Convection and Grain Transport, *Materialia.* 23 (2022) 101462. <https://doi.org/10.2139/ssrn.4053428>.
 23. H. Jung, N. Mangelinck-Noël, H. Nguyen-Thi, N. Bergeon, B. Billia, A. Buffet, G. Reinhart, T. Schenk, J. Baruchel, Fragmentation in an Al–7 wt-%Si alloy studied in real time by X-ray synchrotron techniques, *Int. J. Cast Met. Res.* 22 (2009) 208–211. <https://doi.org/10.1179/136404609X367731>.
 24. N. Shevchenko, S. Boden, G. Gerbeth, S. Eckert, Chimney Formation in Solidifying Ga-25wt pct In Alloys Under the Influence of Thermosolutal Melt Convection, *Met. Mater. Trans. A.* 44 (2013) 3797–3808. <https://doi.org/10.1007/s11661-013-1711-1>.
 25. S. Karagadde, L. Yuan, N. Shevchenko, S. Eckert, P.D. Lee, 3-D microstructural model of freckle formation validated using in situ experiments, *Acta Mater.* 79 (2014) 168–180. <https://doi.org/10.1016/j.actamat.2014.07.002>.
 26. G. Reinhart, H. Nguyen-Thi, N. Mangelinck-Noël, J. Baruchel, B. Billia, In situ investigation of dendrite deformation during upward solidification of Al-7wt.%Si, *JOM.* 66 (2014) 1408–14. <https://doi.org/10.1007/s11837-014-1030-z>.
 27. N. Shevchenko, O. Roshchupkina, O. Sokolova, S. Eckert, The effect of natural and forced melt convection on dendritic solidification in Ga-In alloys, *J. Cryst. Growth.* 417 (2015) 1–8. <https://doi.org/10.1016/j.jcrysgro.2014.11.043>.
 28. A. Ludwig, G. Shayesteh, M. Stefan-Kharicha, M. Wu, A. Kharicha, Interplay of flow stratification, segregation channels, and crystal dynamics in a solidifying aqueous ammonium chloride solution, *Int. J. Heat Mass Transf.* 240 (2025) 126638. <https://doi.org/10.1016/j.ijheatmasstransfer.2024.126638>.

Disclaimer/Publisher's Note: The statements, opinions and data contained in all publications are solely those of the individual author(s) and contributor(s) and not of the publisher and/or the editor(s). This publisher and/or the editor(s) disclaim responsibility for any injury to people or property resulting from any ideas, methods, instructions or products referred to in the content.

© Copyright (2025): Author(s). The licensee is the publisher (BP International).

Peer-Review History:

This chapter was reviewed by following the Advanced Open Peer Review policy. This chapter was thoroughly checked to prevent plagiarism. As per editorial policy, a minimum of two peer-reviewers reviewed the manuscript. After review and revision of the manuscript, the Book Editor approved the manuscript for final publication. Peer review comments, comments of the editor(s), etc. are available here: <https://peerreviewarchive.com/review-history/3590.1>